Ain Shams Engineering Journal 13 (2022) 101615

Contents lists available at ScienceDirect

Ain Shams Engineering Journal

journal homepage: www.sciencedirect.com

Effects of partially supported elastic foundation on free vibration of FGP plates using ES-MITC3 elements

Phu-Cuong Nguyen [a], Quoc Hoa Pham [a,*], Trung Thanh Tran [b], Trung Nguyen-Thoi [c,d,1]

[a] Advanced Structural Engineering Laboratory, Faculty of Civil Engineering, Ho Chi Minh City Open University, Ho Chi Minh City, Viet Nam
[b] Faculty of Mechanical Engineering, Le Quy Don Technical University, Hanoi, Viet Nam
[c] Division of Computational Mathematics and Engineering, Institute for Computational Science, Ton Duc Thang University, Ho Chi Minh City, Viet Nam
[d] Faculty of Civil Engineering, Ton Duc Thang University, Ho Chi Minh City, Viet Nam

ARTICLE INFO

Article history:
Received 6 March 2021
Revised 21 September 2021
Accepted 15 October 2021
Available online 01 November 2021

Keywords:
ES-FEM
Mixed interpolation of tensorial components
Free vibration
Functionally Graded Porous materials (FGP)
Partially supported foundation
Winkler-Pasternak foundation
Plates

ABSTRACT

The main goal of this article further extends the ES-MITC3 element based on first-order shear deformation theory (FSDT) for the free vibration analysis of functionally graded porous (FGP) plates resting on the partially supported elastic foundation (PSEF). The ES-MITC3 element is the union between the mixed interpolation of tensorial components (MITC) technique and an edge-based smoothed finite element method (ES-FEM). The elastic foundation (EF) is a Winkler-Pasternak's model with two parameters consisting of Winkler-stiffness (k_1) and Pasternak-stiffness (k_2). The porosity distribution in plates is assumed to vary according to the even distribution (case 1) and uneven distribution (case 2) rules. The governing equation is derived from Hamilton's principle. Numerical examples are performed to verify the accuracy and reliability of the present method. In addition, the effects of types of PSEF, material properties and geometry characteristics on the free vibration behavior of FGP plates are fully investigated.

1. Introduction

1.1. Overview of analysis of structures made by functionally graded porous materials

Nowadays, the investigation of functionally graded porous (FGP) materials has been concerned by many scientists, including researchers in the material engineering field. In general, the FGP material is a form of FG material with the appearance of internal porosity. Case studies of the mechanical behavior of FG structures can be found in documents [1-8]. Most studies are shown that the increase of the porosity leads to the structural stiffness reduces. However, with outstanding features such as lightweight, excellent energy-absorbing capability, great thermal resistant properties, etc., they have been widely applied in several fields including aerospace, automotive industry, and civil engineering. Some typical works studying FGP structures can be summarized as follows: Shahsavari and coworkers [9] proposed a new Quasi-3D theory to calculate the free vibration of FGP plates. Bansal *et al.* [10] used Navier's solution and FEM for the vibration analysis of FGP plates with partially supported boundary conditions (BCs). Zenkour and his colleagues extended a Quasi-3D theory to analyze the static bending [11], free vibration [12], and post-buckling [13] of FGP structures. Besides, the influences of the porosity factor on the static bending of FG sandwich structures are presented in [14]; and those effects on the free vibration and buckling [15]. Heshmati *et al.* [16] used the pseudo-spectral (PS) method based on Chebyshev polynomials to examine the vibration of circular/annular FGP plates. Nguyen and coworkers employed the polygonal-FEM to study the static and dynamic problems of FGP plates [17] and oscillation control [18]. Kumar *et al.* [19] employed a mesh-free approach for free vibration analysis of FGP plates based on a new higher-order shear deformation theory (HSDT). Rezaei [20,21] based on the analytical method (AM) to investigate the free vibration of FGP plates. Zhao and coworkers improved the Fourier method to study the free vibration [22], the dynamic response of

* Corresponding author.
E-mail addresses: cuong.pn@ou.edu.vn, henycuong@gmail.com (P.-C. Nguyen), hoa.pq@ou.edu.vn (Q.H. Pham), nguyenthoitrung@tdtu.edu.vn (T. Nguyen-Thoi).
[1] Co-author.

Peer review under responsibility of Ain Shams University.

Production and hosting by Elsevier

https://doi.org/10.1016/j.asej.2021.10.010
2090-4479/

FGP shells [23]. Furthermore, the influence of porosity distribution on the mechanical behavior of FGP structures can be found in the literature [5,24-36].

1.2. Overview of analysis of structures resting on the elastic foundation (EF)

The analysis of structures located on the EF can be included in some typical works such as Li *et al.* [37] examined the nonlinear vibration of FGP sandwich plates using Galerkin and the fourth-order Runge–Kutta methods. Zenkour *et al.* [38] proposed a four-unknown variable plate theory for the vibration analysis of composite/sandwich plates. Duc and his colleagues investigated the nonlinear dynamic problem of FGM plates [39] and FGM shells lying on the EF [40]. Moreover, the numerical results of the mechanical response of FGM structures are shown in his book [41]. Mahmoudi and coworkers [42] used a refined Quasi-3D theory to study the bending of FG sandwich plates resting on the Winkler-Pasternak foundation. Xiang and his colleagues [43] used the analytical solution to examine the vibration of Mindlin plates. Omurtag and coworkers [44] employed the mixed finite element formulation based on gateaux differential to investigate the free vibration of thin plates. Zhou and coworkers [45] employed the Ritz method to study the dynamic response of rectangular thick plates while Ferreira *et al.* [46] used radial basis functions for bending and vibration analysis of rectangular plates. In addition, valuable numerical results about mechanical analysis of structures lying on the elastic foundation can be found in [6,30,47-52] and resting on the viscoelastic foundation are provided in the literature [31,53-55]. Recently, with the analysis of structures placed on the PSEF, Motaghian and partners [56] computed the free vibration of rectangular plates by using the analytical solution while Le et al. [57] employed the finite element formulation based on refined shear deformation theories. It should be noted that the PSEF in these researches is only the rectangle domain because they use the quadrilateral element (Q4) to mesh elements. Therefore, the PSEF with the triangular domain still is the limit. To the authors' knowledge, this problem can be solved by using the weak form quadrature element method (QEM) combined with the generalized finite element formulation, as introduced in [58]. Moreover, it is known that the triangular element is preferred to use for the finite element model because it is easy to mesh even with complex geometric domains with simple calculations and thus it is very suitable for calculating the triangular domain elastic foundation. This prompted us to develop the ES-MITC3 element to calculate FGP plates resting on the PSEF includes the triangular domain.

1.3. Overview of ES-MITC3 element

To enhance the accuracy of classical triangular elements, Liu and his coworkers introduced an edge-based smoothed finite element method (ES-FEM) [59-64]. This approach shows some advanced points for structural analysis, including: (1) the numerical results are better convergent and more accurate than original triangular elements; (2) this method also works well for free vibration and dynamic analysis, etc. Recently, the idea of combining the ES-FEM with the MITC3 element [65] to calculate for structures (plate/shell) has been produced [66-71]. In the formulation of the ES-MITC3 element, the stiffness matrix is obtained by using the strain smoothing technique. It can be seen that using the ES-MITC3 element has some interesting advantages in the analysis of the mechanical behavior of structures such as (1) using the ES-MITC3 element can avoid the "shear locking" phenomenon even with very thin plates; (2) using the ES-MITC3 element is better convergent than other elements such as original MITC3 element [65], CS-DSG3 element [72], DSG3 element [73], and more flexible than MITC4 element with the same set nodes [74]. Besides, the ES-FEM has also been combined with *n*-sided polygonal elements [75], using for piezoelectric problems [61], visco-elastoplastic problems [60], and other applications [76-80].

1.4. Novelty of the paper

From the analysis of the above documents, the free vibration study of FGP plates placed on the PSEF using the ES-MITC3 element has not been published yet. So it motivates us to conduct work to fill this gap. The advantage of our work is that for the first time the free vibration of FGP plates partially placed on an elastic foundation including both rectangular and triangular domains is introduced. In addition, the numerical and graphical results indicate that types of PSEF, material properties and geometrical dimensions significantly affect the free vibration of the FGP plate.

1.5. The arrangement of the article

For the convenience of readers, this article is arranged as follows: Section 1 is a general introduction. Section 2 presents the computational model and assumptions. We introduce the finite element formulation for the FGP plate resting on PSEF in Sections 3 and 4. Section 5 is established to verify the accuracy of the present method. The numerical results of free vibration are investigated in Section 6. Finally, some significant conclusions are shown in Section 7.

2. Computational model and assumptions

In this research, we consider a rectangular FGP plate with the length a, the width b and the thickness h resting on the EF as shown in Fig. 1. The PSEF consists of three types: Type 1: The PSEF with the rectangular domain following vertical direction as Fig. 2 (a); Type 2: The PSEF with the rectangular domain following horizontal direction as Fig. 2(b); Type 3: The PSEF with the triangular domain following diagonal line as Fig. 2(c). Note that the area of elastic foundation in all types is the same.

The FGP materials with the variation of two components through-thickness of plates and two different porosity distributions are determined as follows [9]:

$$\text{Case1}: P(z) = P_b + (P_t - P_b)\left(\frac{z}{h} + 0.5\right)^k - \frac{\xi}{2}(P_t + P_b) \tag{1}$$

$$\text{Case2}: P(z) = P_b + (P_t - P_b)\left(\frac{z}{h} + 0.5\right)^k - \frac{\xi}{2}(P_t + P_b)\left(1 - \frac{2|z|}{h}\right) \tag{2}$$

with P represents the effective material properties such as Young's modulus E, mass density ρ. Case 1 and case 2 are respectively the modified mixture rule for the two components with even porosity and uneven porosity. Symbols "b" and "t" denote the typical material properties at the bottom and top surfaces of the plate, respectively. k is the power-law index while ξ ($\xi \leq 1$) represents the porosity factor. It is noted that Poisson's ratio υ is assumed to be constant.

The Winkler-Pasternak foundation is given by [38]:

$$q_e = k_1 w - k_2\left(\frac{\partial^2 w}{\partial x^2} + \frac{\partial^2 w}{\partial y^2}\right) \tag{3}$$

with w is the displacement of the plate along the z-axis; k_1, k_2 are Winkler-stiffness and Pasternak-stiffness, respectively.

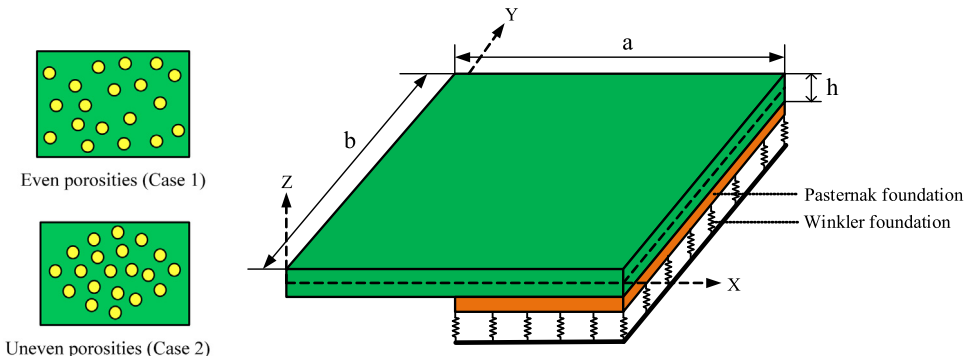

Fig. 1. Model of FGP plates on the PSEF.

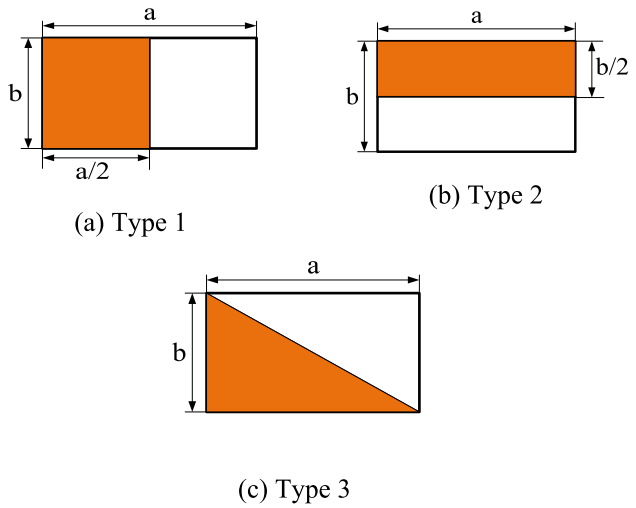

Fig. 2. Different types of PSEF for FGP plates.

3. Finite element method for the FGP plate

The displacement field of FGP plates according to FSDT is determined by [81]:

$$\begin{cases} u(x,y,z) = u_0(x,y) + z\theta_x(x,y) \\ v(x,y,z) = v_0(x,y) + z\theta_y(x,y) \\ w(x,y,z) = w_0(x,y) \end{cases} \tag{4}$$

in which u_0, v_0, w_0, θ_x, θ_y are five-unknown displacements of mid-surface of the plate.

The strain components are expressed as:

$$\boldsymbol{\varepsilon} = \boldsymbol{\varepsilon}_m + z\boldsymbol{\kappa} \tag{5}$$

in which

The membrane strain is:

$$\boldsymbol{\varepsilon}_m = \begin{Bmatrix} u_{0,x} \\ v_{0,y} \\ u_{0,y} + v_{0,x} \end{Bmatrix}; \tag{6}$$

The bending strain is:

$$\boldsymbol{\kappa} = \begin{Bmatrix} \theta_{x,x} \\ \theta_{y,y} \\ \theta_{x,y} + \theta_{y,x} \end{Bmatrix} \tag{7}$$

And the transverse shear strain is:

$$\boldsymbol{\gamma} = \begin{Bmatrix} w_{0,x} + \theta_x \\ w_{0,y} + \theta_y \end{Bmatrix} \tag{8}$$

The stress–strain relations of the plate (Hooke's law) as follows:

$$\begin{Bmatrix} \sigma_x \\ \sigma_y \\ \tau_{xy} \\ \tau_{xz} \\ \tau_{yz} \end{Bmatrix} = \begin{bmatrix} Q_{11} & Q_{12} & 0 & 0 & 0 \\ Q_{21} & Q_{22} & 0 & 0 & 0 \\ 0 & 0 & Q_{66} & 0 & 0 \\ 0 & 0 & 0 & Q_{55} & 0 \\ 0 & 0 & 0 & 0 & Q_{44} \end{bmatrix} \begin{Bmatrix} \varepsilon_x \\ \varepsilon_y \\ \gamma_{xy} \\ \gamma_{xz} \\ \gamma_{yz} \end{Bmatrix} \tag{9}$$

where

$$Q_{11} = Q_{22} = \frac{E(z)}{1-\upsilon^2}; Q_{12} = Q_{21} = \frac{\upsilon E(z)}{1-\upsilon^2}$$

$$Q_{44} = Q_{55} = Q_{66} = \frac{E(z)}{2(1+\upsilon)} \tag{10}$$

Applying Hamilton's principle, motion equations of the FGP plate is obtained as follows [81]:

$$\int_{t_1}^{t_2} (\delta\mathcal{U} - \delta\mathcal{K})\mathrm{d}t = 0 \tag{11}$$

where

The strain energy is:

$$\mathcal{U} = \mathcal{U}^p + \mathcal{U}^f \tag{12}$$

with $\mathcal{U}^f$ is the strain energy of the foundation:

$$\mathcal{U}^f = \frac{1}{2}\int_{\psi} \left(k_1 w^2 - k_2 \left[\left(\frac{\partial^2 w}{\partial x^2}\right)^2 + \left(\frac{\partial^2 w}{\partial y^2}\right)^2 \right] \right) \mathrm{d}\psi \tag{13}$$

and $\mathcal{U}^p$ is the strain energy of the plate:

$$\mathcal{U}^p = \frac{1}{2}\int_{\psi} (\boldsymbol{\varepsilon}^T \boldsymbol{D}\boldsymbol{\varepsilon} + \boldsymbol{\gamma}^T \boldsymbol{C}\boldsymbol{\gamma})\mathrm{d}\psi \tag{14}$$

in which $\boldsymbol{\varepsilon} = [\boldsymbol{\varepsilon}_m \quad \boldsymbol{\kappa}]^T$ and

$$\boldsymbol{D} = \begin{bmatrix} \boldsymbol{A} & \boldsymbol{B} \\ \boldsymbol{B} & \boldsymbol{F} \end{bmatrix} \tag{15}$$

with $\boldsymbol{A}$, $\boldsymbol{B}$, $\boldsymbol{F}$, and $\boldsymbol{C}$ are the component stiffness matrices expressed by

$$(\boldsymbol{A}, \boldsymbol{B}, \boldsymbol{F}) = \int_{-h/2}^{h/2} (1, z, z^2) \begin{bmatrix} Q_{11} & Q_{12} & 0 \\ Q_{21} & Q_{22} & 0 \\ 0 & 0 & Q_{66} \end{bmatrix} \mathrm{d}z \tag{16}$$

$$\boldsymbol{C} = \int_{-h/2}^{h/2} \begin{bmatrix} Q_{55} & 0 \\ 0 & Q_{44} \end{bmatrix} dz \tag{17}$$

The kinetic energy is:

$$\mathcal{K} = \frac{1}{2}\int_{\psi} \dot{\boldsymbol{u}}^T \mathbf{m}_{\mathrm{p}} \dot{\boldsymbol{u}} \mathrm{d}\psi \tag{18}$$

in which $\boldsymbol{u}^T = [\,u_0 \quad v_0 \quad w_0 \quad \theta_x \quad \theta_y\,]$, and $\mathbf{m}_{\mathrm{p}}$ is the inertial matrix defined by:

$$\mathbf{m}_{\mathrm{p}} = \begin{bmatrix} I_1 & 0 & 0 & I_2 & 0 \\ & I_1 & 0 & 0 & I_2 \\ & & I_1 & 0 & 0 \\ & & & I_3 & 0 \\ & & & & I_3 \end{bmatrix} \tag{19}$$

with

$$(I_1, I_2, I_3) = \int_{-h/2}^{h/2} \rho\left(1, z, z^2\right) \mathrm{d}z \tag{20}$$

Substituting Eqs. (13), (18) into Eq. (11), the weak formulation for free vibration analysis of the FGP plate is as follows [81]:

$$\begin{aligned} &\int_{\psi} \delta\boldsymbol{\varepsilon}^T \boldsymbol{D} \boldsymbol{\varepsilon} \mathrm{d}\psi + \int_{\psi} \delta\boldsymbol{\gamma}^T \boldsymbol{C} \boldsymbol{\gamma} \mathrm{d}\psi \\ &+ \int_{\psi} \delta\boldsymbol{w}^T \left[k_1 w - k_2 \left(\frac{\partial^2 w}{\partial x^2} + \frac{\partial^2 w}{\partial y^2} \right) \right] \mathrm{d}\psi \\ &= \int_{\psi} \dot{\boldsymbol{u}}^T \mathbf{m}_{\mathrm{p}} \dot{\boldsymbol{u}} \mathrm{d}\psi \end{aligned} \tag{21}$$

4. An ES-MITC3 method for free vibration problem

4.1. Brief on the MITC3 formulation

The middle surface of the plate (ψ) is divided into n^e finite three-node triangular elements with n^n nodes such that $\psi \approx \sum_{e=1}^{n^e} \psi_e$ and $\psi_i \cap \psi_j = \varnothing, i \neq j$. Then the displacement at any point $\boldsymbol{u}^e = \left[u_j^e, v_j^e, w_j^e, \theta_{xj}^e, \theta_{yj}^e\right]^T$ of element ψ_e is approximated as follows:

$$\boldsymbol{u}^e(\boldsymbol{x}) = \sum_{j=1}^{n^{ne}} \begin{bmatrix} N_I(\mathrm{x}) & 0 & 0 & 0 & 0 \\ 0 & N_I(\mathrm{x}) & 0 & 0 & 0 \\ 0 & 0 & N_I(\mathrm{x}) & 0 & 0 \\ 0 & 0 & 0 & N_I(\mathrm{x}) & 0 \\ 0 & 0 & 0 & 0 & N_I(\mathrm{x}) \end{bmatrix} \boldsymbol{d}_j^e = \sum_{j=1}^{n^{ne}} \boldsymbol{N}(\boldsymbol{x}) \boldsymbol{d}_j^e \tag{22}$$

where n^{ne} is the total number of nodes of ψ_e ; $\boldsymbol{N}(\boldsymbol{x})$ is the shape function matrix; and $\boldsymbol{d}_j^e = \left[u_j^e, v_j^e, w_j^e, \theta_{xj}^e, \theta_{yj}^e\right]^T$ is the degrees of freedom (dof) of nodes.

Membrane bending strains of the MITC3 element are defined by [64]:

$$\boldsymbol{\varepsilon}_m^e = \left[\boldsymbol{B}_{m1}^e \quad \boldsymbol{B}_{m2}^e \quad \boldsymbol{B}_{m3}^e\right] \boldsymbol{d}^e = \boldsymbol{B}_m^e \boldsymbol{d}^e \tag{23}$$

$$\boldsymbol{\kappa}^e = \left[\boldsymbol{B}_{b1}^e \quad \boldsymbol{B}_{b2}^e \quad \boldsymbol{B}_{b3}^e\right] \boldsymbol{d}^e = \boldsymbol{B}_b^e \boldsymbol{d}^e \tag{24}$$

where

$$\boldsymbol{B}_{m1}^e = \frac{1}{2A_e} \begin{bmatrix} b-c & 0 & 0 & 0 & 0 \\ 0 & d-a & 0 & 0 & 0 \\ d-a & b-c & 0 & 0 & 0 \end{bmatrix}, \tag{25}$$

$$\boldsymbol{B}_{m2}^e = \frac{1}{2A_e} \begin{bmatrix} c & 0 & 0 & 0 & 0 \\ 0 & -d & 0 & 0 & 0 \\ -d & c & 0 & 0 & 0 \end{bmatrix}, \tag{26}$$

$$\boldsymbol{B}_{m3}^e = \frac{1}{2A_e} \begin{bmatrix} -b & 0 & 0 & 0 & 0 \\ 0 & a & 0 & 0 & 0 \\ a & -b & 0 & 0 & 0 \end{bmatrix}, \tag{27}$$

$$\boldsymbol{B}_{b1}^e = \frac{1}{2A_e} \begin{bmatrix} 0 & 0 & 0 & b-c & 0 \\ 0 & 0 & 0 & 0 & d-a \\ 0 & 0 & 0 & d-a & b-c \end{bmatrix}, \tag{28}$$

$$\boldsymbol{B}_{b2}^e = \frac{1}{2A_e} \begin{bmatrix} 0 & 0 & 0 & c & 0 \\ 0 & 0 & 0 & 0 & -d \\ 0 & 0 & 0 & -d & c \end{bmatrix}, \tag{29}$$

$$\boldsymbol{B}_{b3}^e = \frac{1}{2A_e} \begin{bmatrix} 0 & 0 & 0 & -b & 0 \\ 0 & 0 & 0 & 0 & a \\ 0 & 0 & 0 & a & -b \end{bmatrix}, \tag{30}$$

To overcome the shear locking phenomenon when the thickness-to-length ratio of the plate becomes very small. The authors employ the formulation of the transverse shear strains of the MITC3 element based on the FSDT to approximate the strain field of plates and can be determined as follows [64]:

$$\boldsymbol{\gamma}^e = \boldsymbol{B}_s^e \boldsymbol{d}^e \tag{31}$$

in which

$$\boldsymbol{B}_s^e = \left[\boldsymbol{B}_{s1}^e \quad \boldsymbol{B}_{s2}^e \quad \boldsymbol{B}_{s3}^e\right] \tag{32}$$

with

$$\boldsymbol{B}_{s1}^e = \boldsymbol{J}^{-1} \begin{bmatrix} 0 & 0 & -1 & \frac{a}{3}+\frac{d}{6} & \frac{b}{3}+\frac{c}{6} \\ 0 & 0 & -1 & \frac{d}{3}+\frac{a}{6} & \frac{c}{3}+\frac{b}{6} \end{bmatrix} \tag{33}$$

$$\boldsymbol{B}_{s2}^e = \boldsymbol{J}^{-1} \begin{bmatrix} 0 & 0 & 1 & \frac{a}{2}-\frac{d}{6} & \frac{b}{2}-\frac{c}{6} \\ 0 & 0 & 0 & \frac{d}{6} & \frac{c}{6} \end{bmatrix} \tag{34}$$

$$\boldsymbol{B}_{s3}^{e(0)} = \boldsymbol{J}^{-1} \begin{bmatrix} 0 & 0 & 0 & \frac{a}{6} & \frac{b}{6} \\ 0 & 0 & 1 & \frac{d}{2}-\frac{a}{6} & \frac{c}{2}-\frac{b}{6} \end{bmatrix} \tag{35}$$

where

$$\boldsymbol{J}^{-1} = \frac{1}{2A_e} \begin{bmatrix} c & -b \\ -d & a \end{bmatrix} \tag{36}$$

in which $a = x_2 - x_1$, $b = y_2 - y_1$, $c = y_3 - y_1$, $d = x_3 - x_1$, and A_e is the area of a triangular element domain (see Fig. 3).

Substituting displacement fields into Eq. (21), the governing equation for free vibration analysis of FGP plates resting on the EF is obtained as follows:

$$(\boldsymbol{K} - \omega^2 \boldsymbol{M}) \boldsymbol{d} = 0 \tag{37}$$

in which

The stiffness matrix is defined by:

$$\boldsymbol{K} = \sum_{e=1}^{n^e} \left(\boldsymbol{K}_p^e + \boldsymbol{K}_f^e \right), \tag{38}$$

with

$$\boldsymbol{K}_p^e = \int_{\psi_e} \boldsymbol{B}^T \boldsymbol{D} \boldsymbol{B} \mathrm{d}\psi_e + \int_{\psi_e} \boldsymbol{B}_s^T \boldsymbol{C} \boldsymbol{B}_s \mathrm{d}\psi_e \tag{39}$$

and

$$\begin{aligned} \boldsymbol{K}_f^e = k_1 \int_{\psi_e} \mathbf{N}_w^{\mathrm{T}} \mathbf{N}_w \mathrm{d}\psi_e + \mathrm{k}_2 \\ \times \int_{\psi_e} \left[\left(\frac{\partial \mathbf{N}_w}{\partial \mathrm{x}} \right)^{\mathrm{T}} \left(\frac{\partial \mathbf{N}_w}{\partial \mathrm{x}} \right) + \left(\frac{\partial \mathbf{N}_w}{\partial \mathrm{y}} \right)^{\mathrm{T}} \left(\frac{\partial \mathbf{N}_w}{\partial \mathrm{y}} \right) \right] \mathrm{d}\psi_e \end{aligned} \tag{40}$$

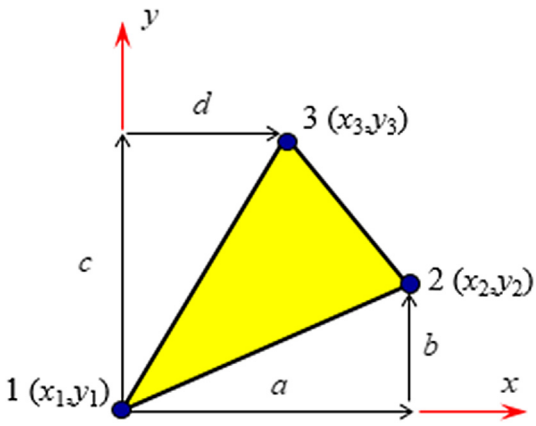

Fig. 3. Node-coordinates of the triangular domain.

where

$$B^e = \begin{bmatrix} B_m^e & B_b^e \end{bmatrix} \tag{41}$$

$$N_w = [0\ 0\ N_1\ 0\ 0,\ 0\ 0\ N_2\ 0\ 0,\ 0\ 0\ N_3\ 0\ 0] \tag{42}$$

The mass matrix is determined as:

$$M = \sum_{e=1}^{n^e} \left(M_p^e + M_f^e \right) \tag{43}$$

with

$$\boldsymbol{M}_p^e = \int_{\psi_e} \boldsymbol{N}^T \boldsymbol{m_p} \boldsymbol{N} \mathrm{d}\psi_e \tag{44}$$

$$\boldsymbol{M}_f^e = \boldsymbol{m_f} \int_{\psi_e} \boldsymbol{N}_w^T \boldsymbol{N}_w \mathrm{d}\psi_e \tag{45}$$

4.2. Brief on the ES-MITC3 formulation

The smoothing domains ψ^k is built relied on edges of the three-node triangular elements such that $\psi = \bigcup_{k=1}^{n^k} \psi^k$ and $\psi_i^k \cap \psi_j^k = \varnothing \text{for} i \neq j$. The edge-based smoothing domain ψ^k for the inner edge k is created by connecting two end-nodes of the edge to the center of adjacent triangular MITC3 elements, as plotted in Fig. 4.

By employing the edge-based smoothing technique in [64], the smoothed membrane, bending, and shear strain $\boldsymbol{\varepsilon_m^k}, \boldsymbol{\kappa^k}, \boldsymbol{\gamma^k}$ over the smoothing domain $\psi^{\boldsymbol{k}}$ can be obtained by:

$$\boldsymbol{\varepsilon}_m^k = \int_{\psi^k} \boldsymbol{\varepsilon}_m \Phi^k(\mathrm{x}) \mathrm{d}\psi, \tag{46}$$

$$\boldsymbol{\kappa}^k = \int_{\psi^k} \boldsymbol{\kappa} \Phi^k(\mathrm{x}) \mathrm{d}\psi, \tag{47}$$

$$\boldsymbol{\gamma}^k = \int_{\psi^k} \boldsymbol{\gamma} \Phi^k(\mathrm{x}) \mathrm{d}\psi, \tag{48}$$

where $\boldsymbol{\varepsilon}_m$, $\boldsymbol{\kappa}$, and $\boldsymbol{\gamma}$ are the compatible membrane, bending, and shear strains, respectively. $\Phi^k(\mathrm{x})$ is the smoothing function such that satisfies at least unity property $\int_{\psi^k} \Phi^k(\mathrm{x}) \mathrm{d}\psi = 1$.

with $\Phi^k(\mathrm{x})$ is determined as follows:

$$\Phi^k(\mathrm{x}) = \begin{cases} \frac{1}{A^k} x \in \psi^k \\ 0 x \notin \psi^k \end{cases} \tag{49}$$

where A^k is the area of the smoothing domain ψ^k :

$$A^k = \int_{\psi^k} \mathrm{d}\psi = \frac{1}{3} \sum_{i=1}^{n^{ek}} A^i \tag{50}$$

with n^{ek} is the total number of the adjacent elements in the smoothing domain ψ^k ; and A^i is the area of the i^{th} triangular element.

By substituting Eqs. (46)–(48) into Eqs. (23)–(24) and (31), the approximation of the smoothed strains is as follows:

$$\varepsilon_m^k = \sum_{j=1}^{n^{nk}} \mathbf{B}_{mj}^k \boldsymbol{d}_j^k; \kappa^k = \sum_{j=1}^{n_{sh}^{nk}} \mathbf{B}_{bj}^k \boldsymbol{d}_j^k; \gamma^k = \sum_{j=1}^{n_{sh}^{nk}} \mathbf{B}_{sj}^k \boldsymbol{d}_j^k \tag{51}$$

where n_{sh}^{nk} is the total number of nodes of the smoothing domain attached to edge k ($n_{sh}^{nk} = 3$ for the smoothing domain with boundary edges and $n_{sh}^{nk} = 4$ for the smoothing domain with inner edges as depicted in Fig. 4; $\boldsymbol{d}_j^k$ is the nodal d.o.f of the smoothing domain ψ^k ; $\mathbf{B}_{mj}^k$, $\mathbf{B}_{bj}^k$, and $\mathbf{B}_{sj}^k$ are respectively the smoothed membrane, bending, and shear strain gradient matrices. The j^{th} node of elements attached to edge k is calculated by [66]:

$$\mathbf{B}_{mj}^k = \frac{1}{A^k} \sum_{i=1}^{n^{ek}} \frac{1}{3} A^i \boldsymbol{B}_{mj}^e \tag{52}$$

$$\boldsymbol{B}_{bj}^k = \frac{1}{A^k} \sum_{i=1}^{n^{ek}} \frac{1}{3} A^i \boldsymbol{B}_{bj}^e \tag{53}$$

$$\boldsymbol{B}_{sj}^k = \frac{1}{A^k} \sum_{i=1}^{n^{ek}} \frac{1}{3} A^i \boldsymbol{B}_{sj}^e \tag{54}$$

Then, the stiffness matrix of the plate is assembled as follows:

$$\mathbf{K} = \sum_{k=1}^{n_{sh}^k} \mathbf{K}^k \tag{55}$$

where $\mathbf{K}^k$ is the stiffness matrix of the smoothing domain ψ^k using the ES-MITC3 element and given by [66]:

$$\boldsymbol{K}^k = \int_{\psi^k} \left(\boldsymbol{B}^{kT} \boldsymbol{D} \boldsymbol{B}^k + \boldsymbol{B}_s^{kT} \boldsymbol{C} \boldsymbol{B}_s^k \right) d\psi = \boldsymbol{B}^{kT} \boldsymbol{D} \boldsymbol{B}^k A^k + \boldsymbol{B}_s^{kT} \boldsymbol{C} \boldsymbol{B}_s^k A^k \tag{56}$$

in which

$$\boldsymbol{B}^{kT} = \begin{bmatrix} \boldsymbol{B}_{mj}^k & \boldsymbol{B}_{bj}^k \end{bmatrix} \tag{57}$$

4.3. Validation of the present method

The main purpose of this section is to perform examples to confirm the convergence and accuracy of the present method. The authors calculate the stiffness and mass matrices of the plate and the foundation independently as formulations presented in Section 4. Then, the plate elements supported by the foundation will have the stiffness matrix added to the stiffness of the foundation element. In this study, non-dimensional factors are introduced by formulation:

$$K_1 = \frac{k_1 a^4}{H}; K_2 = \frac{k_2 a^2}{H}; \omega^* = \frac{\omega a^2}{h} \sqrt{\frac{\rho}{E}} \text{ with } H = \frac{Eh^3}{12(1-\upsilon^2)} \tag{58}$$

To verify the performance of the ES-MITC3 element compared with different methods, the relative frequency error is defined by

$$Er(\%) = 100 \times \frac{\left| \omega_{pr}^* - \omega_{re}^* \right|}{\left| \omega_{re}^* \right|} \tag{59}$$

where ω_{pr}^* and ω_{re}^* are the non-dimensional natural frequencies of the present method and non-dimensional frequencies of the reference method, respectively.

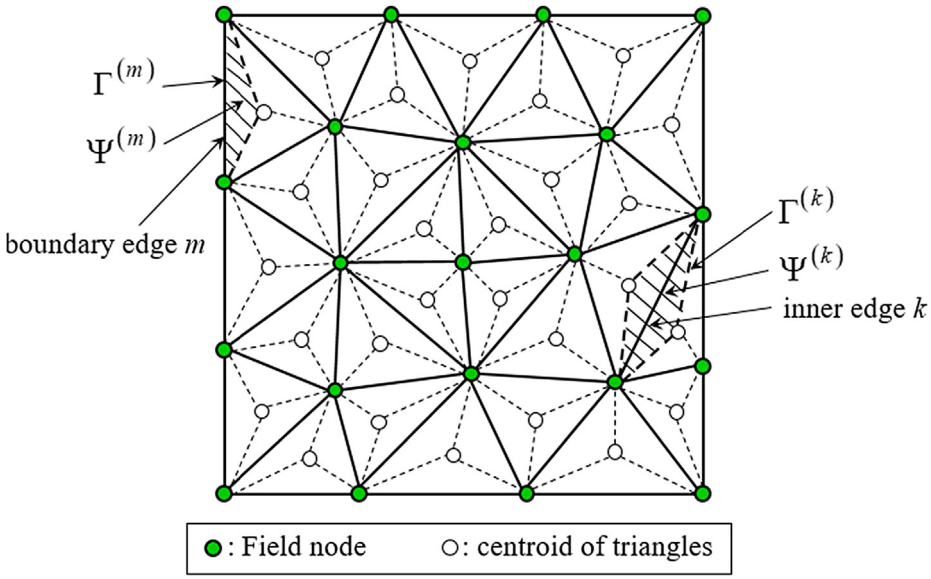

Fig. 4. The smoothing domain $\psi^{\mathbf{k}}$ is created by the triangular elements.

Example 1. Firstly, a SSSS FGP (Al/Al_2O_3) square plate is considered with material properties as $E_b = 70\ GPa$, $\rho_b = 2702\ Kg/m^3$, $E_t = 380\ GPa$, $\rho_t = 3800\ Kg/m^3$ while $\upsilon = 0.3$ is fixed. The stiffness factor and non-dimensional natural frequencies are determined as Eq. (58) with $H_b = \frac{E_b h^3}{12(1-\upsilon^2)}$ and $\omega^* = \frac{\omega a^2}{h}\sqrt{\frac{\rho_b}{E_b}}$. Fig. 5 presents non-dimensional natural frequencies of SSSS FGP plates via different mesh sizes ($n_x \times n_y$). In which n_x and n_y are the total number of nodes on the length and width of the plate, respectively. It can be observed that the non-dimensional natural frequencies converge with the mesh sizes 19×19. From here, the author will use the mesh sizes 19×19 for the next examples.

Next, the first non-dimensional natural frequencies of our work compared with those of Shahsavari et al. [9] using the Quasi-3D theory are listed in Table 1. From this table, it can be concluded that the obtained results are in good agreement with the results of Ref. [9] (errors are less than 1.6%).

Example 2. Secondly, the plates are partially supported by a Winkler foundation [56] as displayed in Fig. 6. Parameters of the isotropic plate as L_x = 2 m, L_y = 1 m, h = 0.01 m, E = 200 GPa, $\upsilon = 0.3$, and $\rho = 7850\ Kg/m^3$. The first non-dimensional natural frequencies as in Eq. (58) of the present work compared to those of *Motaghian et al.* [56] using the analytical solution are listed in Table 2. It can be observed that the numerical results in our work compared to those of Ref. [56] has an error of less than 3%.

From the above two examples, it can be confirmed that the proposed method and the calculation program ensure accuracy and reliability.

5. Numerical results

In this section, the free vibration of (Al/Al_2O_3) plates is considered. The geometry parameters of the FGP plate are $b/a = 2$ (a is fixed) while material properties as metal (Al) $E_m = 70\ GPa$, $\rho_m = 2702\ Kg/m^3$ and ceramic (Al_2O_3) $E_c = 380\ GPa$, $\rho_c = 3800\ Kg/m^3$. Poisson's ratio is constant $\upsilon = 0.3$ and the porosity volume fraction gets value $\xi = 0.5$. The non-dimensional parameters are provided in Eq. (58) with $H_b = \frac{E_b h^3}{12(1-\upsilon^2)}$ and $\omega^* = \frac{\omega a^2}{h}\sqrt{\frac{\rho_b}{E_b}}$.

Fig. 7 presents the first mode shape of the SSSS FGP plates with the different cases of porosity distribution and types of PSEF. It can be found that with the same BCs and the porosity distribution, the maximum value of the first natural frequency of the FGP plate is placed on the PSEF (type 1), and the minimum value of the FGP plate is placed on the PSEF (type 2). Figs. 8–10 show the first six mode shapes of the FGP (case 1) plate resting on the PSEF (type 1) with different BCs. We can also be concluded that the mode shape of the FGP plate is not symmetric because the stiffness at each position of the plate has different values. The maximum displacement of the mode shapes is traveled to the location of the plate not supported by foundations. Additionally, the natural frequencies of the CCCC plate are larger than the SCSC plate and the SSSS plate. This is quite reasonable because the CCCC boundary condition is less flexible than the SCSC and SSSS boundary conditions.

5.1. Effect of the parameters-PSEF

For this purpose, let us change K_1 from 0 to 100, K_2 gets values from 0 to 100, porosity volume fraction $\xi = 0.2$, and power-law index $k = 1$. The first non-dimensional natural frequencies of the FGP plates are listed in Tables 3–6 and plotted in Figs. 11 and 12. From these figures and tables, it can be seen that when foundation stiffness increases, leading to an increase of the first non-dimensional natural frequencies of FGP plates. It is also concluded that the effect of the Pasternak foundation (K_2) is stronger than the Winkler foundation (K_1) for all cases of porosity distributions and types of PSEF. Specifically, with the same geometry parameters and material properties (see Type 1 in Table 3), when $K_2 = 50$ and K_1 increases from 0 to 100, the first non-dimensional natural frequency increases from 7.4973 to 7.7678 (about 3.6%), but when $K_1 = 50$ and K_2 increases from 0 to 100, the first non-dimensional natural frequency increases from 5.5675 to 9.1197 (about 63,8%). Furthermore, the first non-dimensional natural frequency of the CCCC FGP plates is the largest in all boundary conditions.

5.2. Effects of FGP parameters

In this subsection, the influence of material properties on the free vibration of FGP plates are produced. For that purpose, the

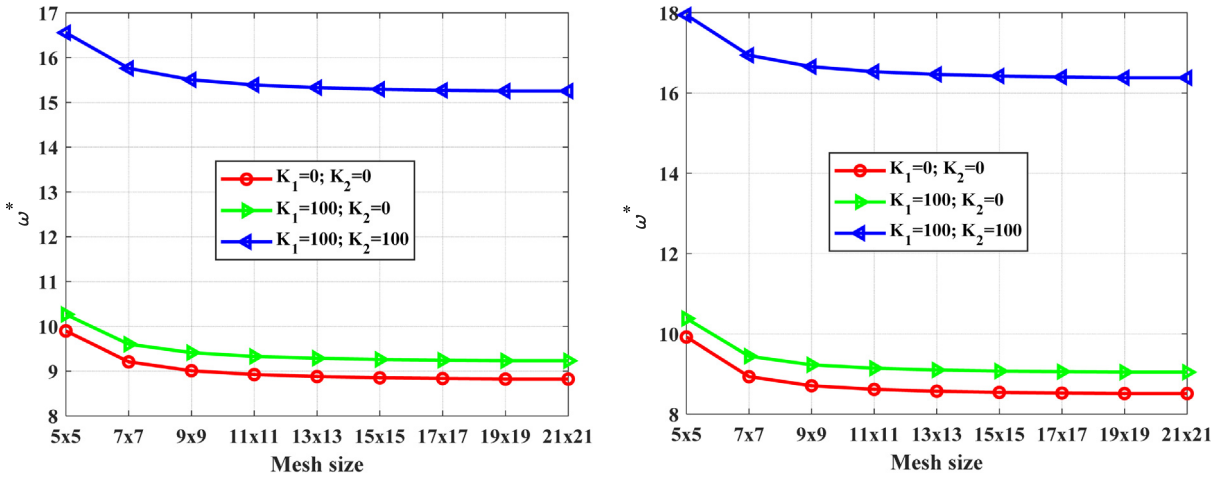

a) The non-dimensional frequency of the FGP plate with $h/a = 0.1$ and $\xi = 0$.

b) The non-dimensional frequency of the FGP plate with $h/a = 0.05$ and $\xi = 0.2$.

Fig. 5. The convergence of mesh size to the non-dimensional frequency of FGP plates.

Table 1
First non-dimensional natural frequencies of FGP plates versus the foundation stiffness (k = 1).

(K_1, K_2)	h/a	$\xi = 0$			$\xi = 0.2$		
		Present	[9]	$Er(\%)$	Present	[9]	$Er(\%)$
(0, 0)	0.05	9.010	9.020	0.11	8.485	8.370	1.37
	0.10	8.823	8.818	0.06	8.319	8.203	1.41
	0.15	8.541	8.516	0.29	8.069	7.950	1.50
	0.20	8.196	8.151	0.55	7.762	7.641	1.58
	0.05	9.389	9.430	0.43	9.020	8.917	1.16
	0.10	9.207	9.231	0.26	8.858	8.753	1.20
(100, 0)	0.15	8.933	8.934	0.01	8.614	8.505	1.28
	0.20	8.599	8.577	0.26	8.315	8.203	1.37
	0.05	15.383	15.439	0.36	16.338	16.320	0.11
	0.10	15.213	15.245	0.21	16.175	16.148	0.17
(100, 100)	0.15	14.962	14.966	0.03	15.932	15.895	0.23
	0.20	14.664	14.640	0.16	15.639	15.595	0.28

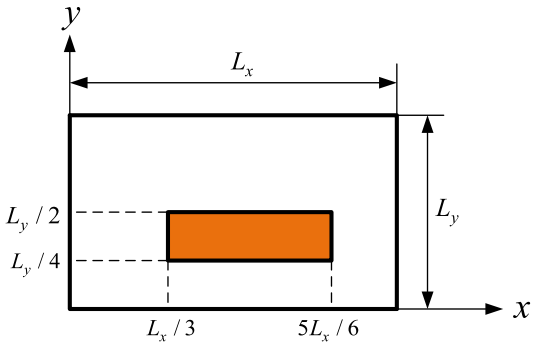

Fig. 6. The plate is partially supported by EF.

power-law index k is chosen in the range from 0 to 10 while the porosity volume fractions ξ gets values from 0 to 0.3, with $\xi = 0$ is the case of the perfect FGP plate. Tables 7–10 and Figs. 13 and 14 show the first non-dimensional natural frequency of the FGP plates resting on the PSEF. From these numerical results, it can be seen that the first non-dimensional natural frequency of the FGP plates depends on material properties and types of PSEF. Specifically, for all types of PSEF and porosity distribution, the first non-dimensional natural frequency of the FGP plates decreases when the power-law index k increases. This problem can be explained by the increase in the ratio of metal in the FGP plates leads to a decrease in the stiffness of plates. When the power-law index $k = 0$, the increase of the porosity volume fractions $\xi$from 0 to 0.3 makes the increase of the first non-dimensional natural frequency of the FGP plates for all cases of porosity distribution. In the case 1 (even porosity) with power-law index $k = 2$, the increase of porosity volume fractions ξlead to the decrease of frequencies of the FGP plates, and when the power-law index $k > 2$, the increase of porosity volume fractions ξ makes the frequencies of the FGP plates decrease rapidly. In the case 2 (uneven porosity), the frequencies of the FGP plates do not change much despite the power-law index $k > 2$. This can be easily observed in Fig. 14. It can also be concluded that it is not easy to predict the general law of natural frequencies when these two parameters change because they affect both the stiffness and the mass of FGP plates.

6. Conclusion

In this article, we have successfully extended the ES-MITC3 element to establish a finite element formulation for the free vibra-

Table 2
Non-dimensional natural frequencies of plates.

Boundary condition (BC)		SSSS (fully simple supported)			CCCC (fully clamped)		
K_1	ω_i^*	Present	[56]	$Er(\%)$	Present	[56]	$Er(\%)$
10	ω_1^*	5.0248	5.003	*0.44*	10.0251	10.295	*2.62*
	ω_2^*	8.089	8.001	*1.10*	13.1172	13.348	*1.73*
	ω_3^*	13.2883	13.00	*2.22*	18.7237	18.782	*0.31*
	ω_4^*	17.1745	17.00	*1.03*	26.2669	26.226	*0.16*
	ω_5^*	20.3426	20.00	*1.71*	29.504	29.853	*1.17*
10^3	ω_1^*	5.3526	5.3100	*0.80*	10.2248	10.481	*2.44*
	ω_2^*	8.2360	8.1300	*1.30*	13.2341	13.451	*1.61*
	ω_3^*	13.3721	13.080	*2.23*	18.7957	18.851	*0.29*
	ω_4^*	17.2364	17.058	*1.05*	26.3223	26.675	*1.32*
	ω_5^*	20.3779	20.064	*1.56*	29.5407	29.886	*1.16*

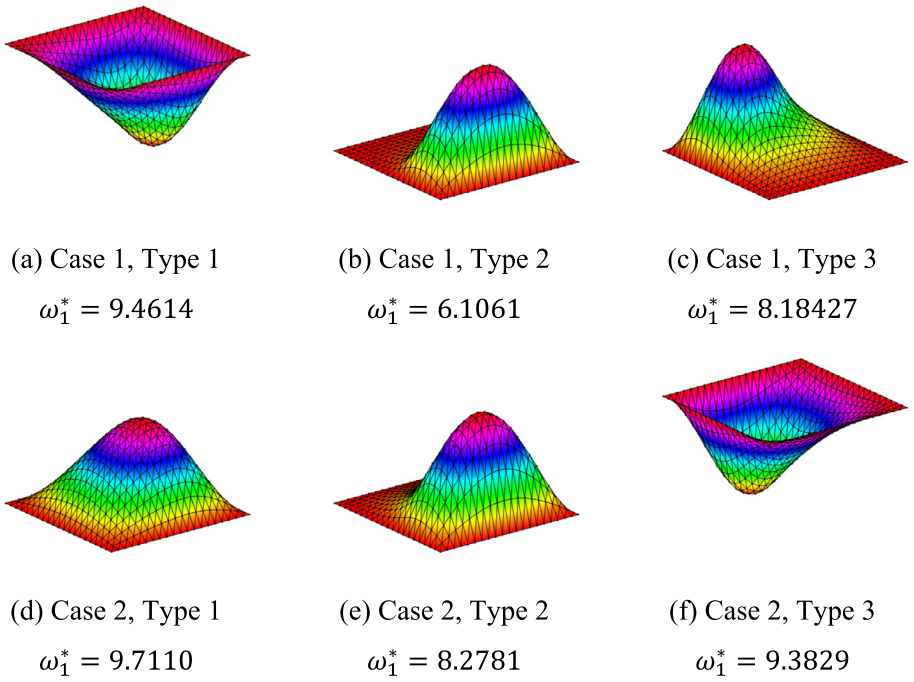

Fig. 7. The first mode shape of SSSS FGP plates with different cases of porosity distribution and types of the PSEF, $k = 1$, $K_1 = 100, K_2 = 100$.

tion analysis of FGP plates located on the PSEF including the triangular domain. Numerical examples are conducted to demonstrate the convergence and accuracy of the present method as well as providing new numerical results on the free vibrations of FGP plates. From obtained results, the main contributions of our work can be summarized as follows:

- The ES-MITC3 uses only triangular elements and thus it is easy and flexible for meshing elements as well as modeling elastic foundation with different shapes including the triangular domain.
- The FGP plates resting on different types of PSEF lead to various natural frequencies. This shows the partially supported foundation significantly affects the free vibration of plates.

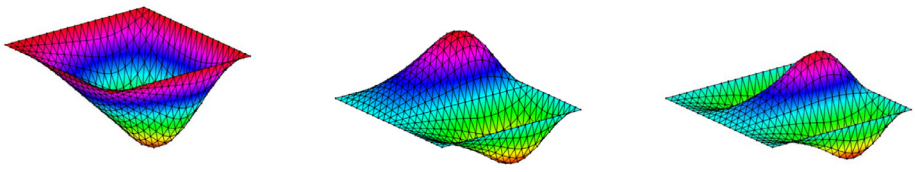

(a) Mode 1 $\omega_1^* = 9.4614$ (b) Mode 2 $\omega_2^* = 11.9675$ (c) Mode 3 $\omega_3^* = 15.8842$

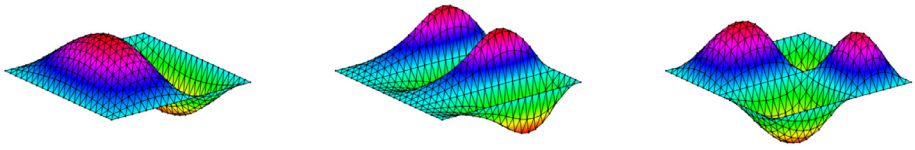

(d) Mode 4 $\omega_4^* = 19.4403$ (e) Mode 5 $\omega_5^* = 21.3885$ (f) Mode 6 $\omega_6^* = 22.6832$

Fig. 8. Mode shapes of the SSSS FGP (case 1) plate lying on the PSEF (type 1), $k = 1$, $K_1 = 100, K_2 = 100$.

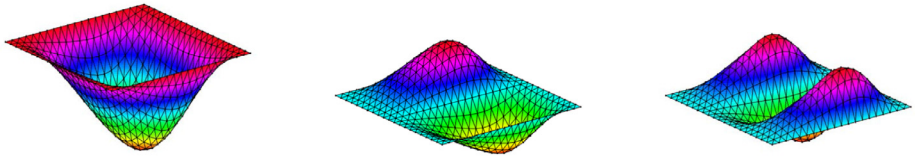

(a) Mode 1 $\omega_1^* = 12.3863$ (b) Mode 2 $\omega_2^* = 14.8242$ (c) Mode 3 $\omega_3^* = 18.6327$

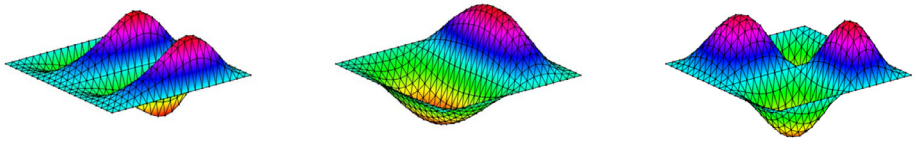

(e) Mode 4 $\omega_4^* = 23.9450$ (f) Mode 5 $\omega_5^* = 25.1834$ (g) Mode 6 $\omega_5^* = 27.8721$

Fig. 9. Mode shapes of the SCSC FGP (case 1) plate lying on the PSEF (type 1), $k = 1$, $K_1 = 100, K_2 = 100$.

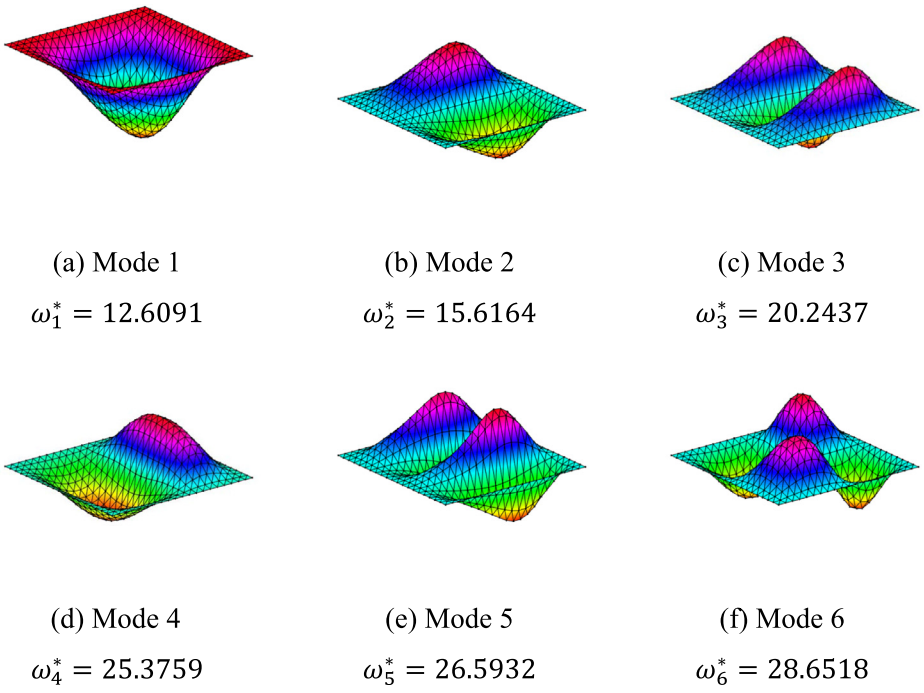

Fig. 10. Mode shapes of the CCCC FGP (case 1) plate lying on the PSEF (type 1), $k = 1, K_1 = 100, K_2 = 100$.

Table 3
Frequencies of SSSS FGP (case 1) plates with different values of K_1 and K_2.

Type of PSEF	K_2	K_1				
		0	25	50	75	100
Type 1	0	5.3530	5.4616	5.5675	5.6708	5.7716
	25	6.5431	6.6267	6.7088	6.7895	6.8688
	50	7.4973	7.5664	7.6344	7.7016	7.7678
	75	8.3068	8.3661	8.4246	8.4824	8.5396
	100	9.0161	9.0681	9.1197	9.1707	9.2212
Type 2	0	5.3530	5.4599	5.5607	5.6558	5.7455
	25	6.3601	6.4168	6.4708	6.5222	6.5712
	50	6.9594	6.9937	7.0267	7.0584	7.0889
	75	7.3663	7.3891	7.4112	7.4326	7.4533
	100	7.6654	7.6816	7.6974	7.7127	7.7276
Type 3	0	5.3530	5.4608	5.5644	5.6640	5.7599
	25	6.5113	6.5876	6.6615	6.7331	6.8027
	50	7.3968	7.4552	7.5121	7.5675	7.6215
	75	8.1168	8.1634	8.2089	8.2533	8.2966
	100	8.7214	8.7594	8.7966	8.8330	8.8685

Table 4
Frequencies of CCCC FGP (case 1) plates with different values of K_1 and K_2.

Type of PSEF	K_2	K_1				
		0	25	50	75	100
Type 1	0	10.6931	10.7480	10.8024	10.8564	10.9101
	25	11.4867	11.5365	11.5860	11.6352	11.6840
	50	12.2102	12.2560	12.3016	12.3468	12.3918
	75	12.8772	12.9197	12.9619	13.0040	13.0458
	100	13.4973	13.5370	13.5765	13.6158	13.6549
Type 2	0	10.6931	10.7475	10.8004	10.8520	10.9022
	25	11.3963	11.4342	11.4711	11.5070	11.5420
	50	11.9073	11.9345	11.9610	11.9869	12.0122
	75	12.2957	12.3159	12.3357	12.3550	12.3739
	100	12.6020	12.6175	12.6327	12.6475	12.6621
Type 3	0	10.6931	10.7477	10.8015	10.8543	10.9063
	25	11.4683	11.5145	11.5599	11.6047	11.6488
	50	12.1463	12.1861	12.2253	12.2640	12.3021
	75	12.7492	12.7839	12.8181	12.8519	12.8852
	100	13.2912	13.3217	13.3519	13.3816	13.4110

Table 5
Frequencies of SSSS FGP (case 2) plates with different values of K_1 and K_2.

Type of PSEF	K_2	K_1				
		0	25	50	75	100
Type 1	0	5.7308	5.8211	5.9097	5.9965	6.0817
	25	6.7452	6.8183	6.8903	6.9613	7.0313
	50	7.5894	7.6516	7.7130	7.7736	7.8336
	75	8.3214	8.3758	8.4296	8.4829	8.5356
	100	8.9723	9.0208	9.0689	9.1166	9.1638
Type 2	0	5.7308	5.8200	5.9052	5.9867	6.0647
	25	6.6177	6.6716	6.7233	6.7730	6.8208
	50	7.1954	7.2308	7.2650	7.2981	7.3301
	75	7.6081	7.6330	7.6571	7.6806	7.7033
	100	7.9217	7.9400	7.9579	7.9753	7.9923
Type 3	0	5.7308	5.8206	5.9077	5.9921	6.0740
	25	6.7233	6.7913	6.8576	6.9222	6.9853
	50	7.5182	7.5727	7.6260	7.6781	7.7291
	75	8.1847	8.2297	8.2739	8.3171	8.3595
	100	8.7584	8.7963	8.8336	8.8702	8.9060

Table 6
Frequencies of CCCC FGP (case 2) plates with different values of K_1 and K_2.

Type of PSEF	K_2	K_1				
		0	25	50	75	100
Type 1	0	11.4451	11.4907	11.5359	11.5809	11.6257
	25	12.1104	12.1526	12.1946	12.2364	12.2779
	50	12.7283	12.7678	12.8070	12.8461	12.8850
	75	13.3065	13.3436	13.3805	13.4173	13.4539
	100	13.8507	13.8858	13.9207	13.9554	13.9900
Type 2	0	11.4451	11.4903	11.5346	11.5781	11.6206
	25	12.0497	12.0837	12.1171	12.1498	12.1818
	50	12.5176	12.5437	12.5693	12.5944	12.6190
	75	12.8904	12.9108	12.9309	12.9506	12.9699
	100	13.1950	13.2113	13.2273	13.2430	13.2585
Type 3	0	11.4451	11.4905	11.5353	11.5795	11.6232
	25	12.0981	12.1379	12.1771	12.2160	12.2543
	50	12.6846	12.7199	12.7548	12.7892	12.8233
	75	13.2175	13.2491	13.2803	13.3112	13.3417
	100	13.7056	13.7340	13.7622	13.7900	13.8176

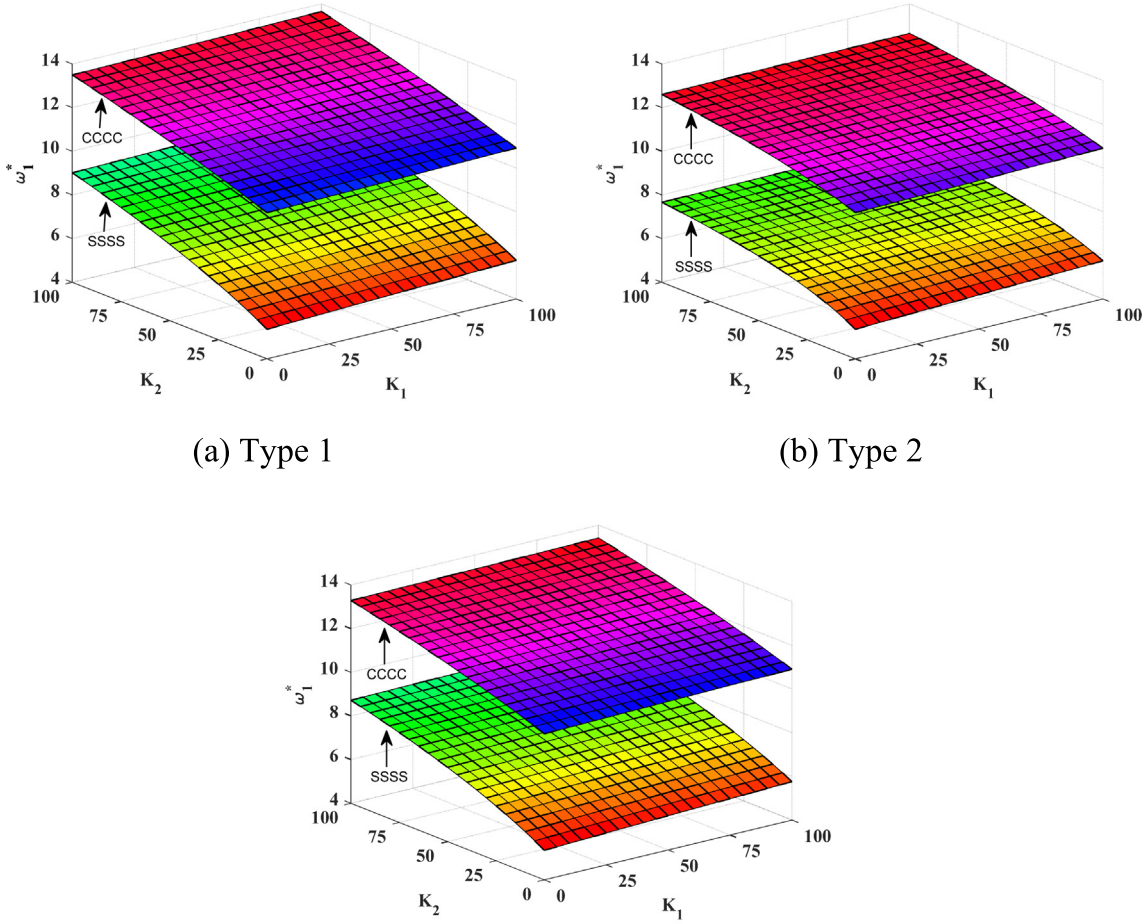

Fig. 11. Frequencies of FGP (case 1) plates with different values of K_1 and K_2. (a) Type 1, (b) Type 2, (c) Type 3.

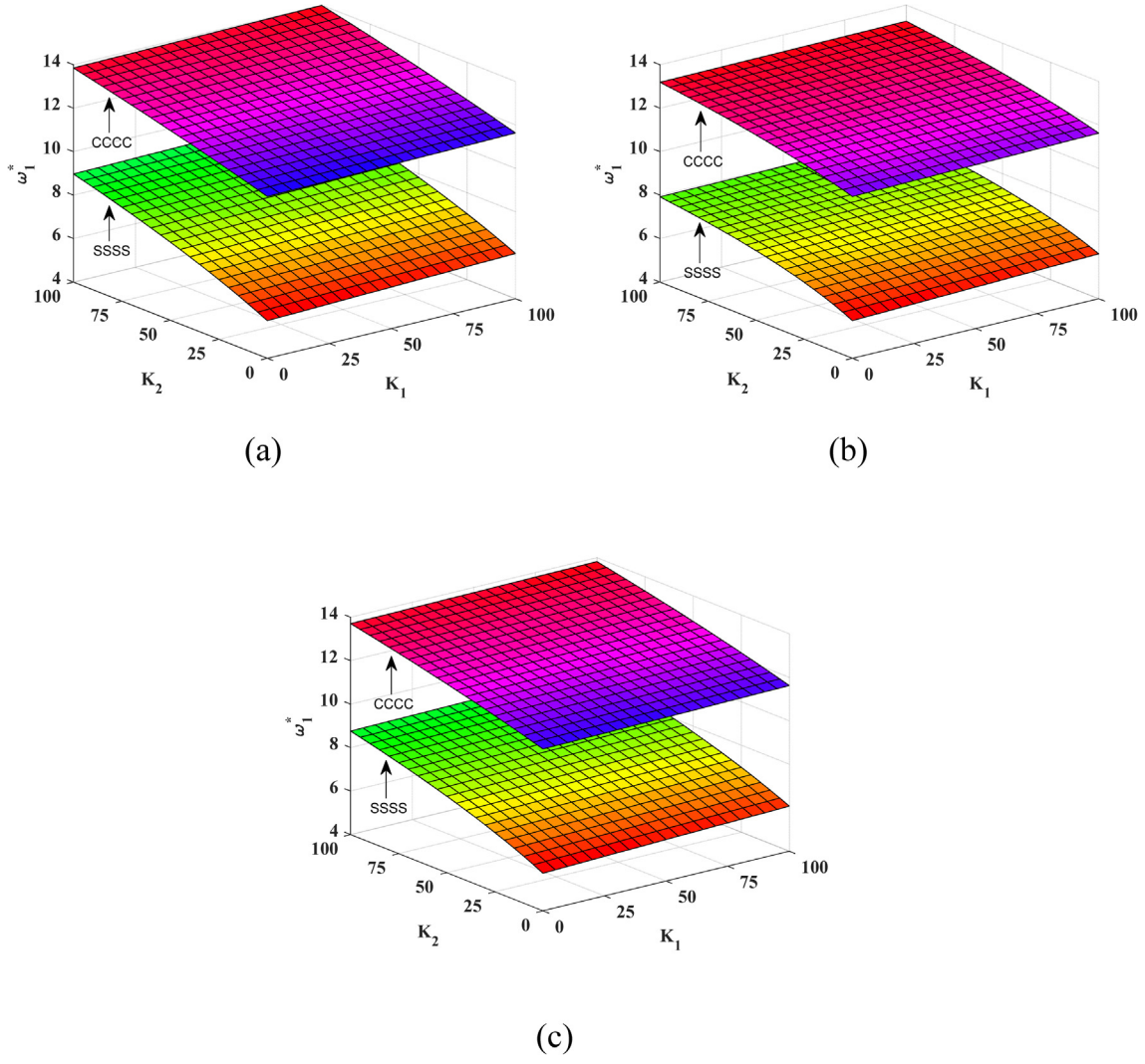

Fig. 12. Frequencies of FGP (case 2) plates with different values of K_1 and K_2. (a) Type 1, (b) Type 2, (c) Type 3.

Table 7
Frequencies of SSSS FGP (Case 1) plates versus k and ξ ($K_1 = 100, K_2 = 10$).

Type of PSEF	ξ	k				
		0	1	2	5	10
Type 1	0	6.4003	5.1731	4.8447	4.7018	4.6186
	0.06	6.4678	5.1582	4.7829	4.6183	4.5471
	0.12	6.5422	5.1373	4.7004	4.4999	4.4445
	0.18	6.6246	5.1082	4.5876	4.3232	4.2858
	0.24	6.7164	5.0672	4.4282	4.0372	4.0070
	0.30	6.8194	5.0091	4.1914	3.4792	3.3108
Type 2	0	6.3418	5.1561	4.8379	4.6995	4.6179
	0.06	6.4105	5.1449	4.7796	4.6182	4.5470
	0.12	6.4862	5.1279	4.6999	4.4987	4.4408
	0.18	6.5700	5.1025	4.5871	4.3108	4.2658
	0.24	6.6633	5.0650	4.4200	3.9735	3.9185
	0.30	6.7679	5.0090	4.1494	3.0409	2.5783
Type 3	0	6.3647	5.1563	4.8333	4.6934	4.6117
	0.06	6.4325	5.1431	4.7737	4.6122	4.5421
	0.12	6.5072	5.1241	4.6936	4.4959	4.4412
	0.18	6.5900	5.0970	4.5831	4.3202	4.2825
	0.24	6.6822	5.0583	4.4252	4.0293	3.9956
	0.30	6.7855	5.0026	4.1861	3.3955	3.1228

Table 8
Frequencies of CCCC FGP (Case 1) plates versus k and ξ ($K_1 = 100, K_2 = 10$).

Type of PSEF	ξ	k				
		0	1	2	5	10
Type 1	0	12.1780	9.4730	8.7037	8.3214	8.1013
	0.06	12.2876	9.3863	8.5004	8.0550	7.8534
	0.12	12.4087	9.2785	8.2381	7.6912	7.5148
	0.18	12.5430	9.1422	7.8894	7.1649	7.0165
	0.24	12.6930	8.9668	7.4075	6.3330	6.1821
	0.30	12.8615	8.7356	6.7024	4.7602	4.2936
Type 2	0	11.8029	9.2347	8.5091	8.1530	7.9476
	0.06	11.9118	9.1590	8.3240	7.9094	7.7222
	0.12	12.0321	9.0642	8.0843	7.5750	7.4125
	0.18	12.1655	8.9435	7.7643	7.0882	6.9525
	0.24	12.3144	8.7870	7.3196	6.3089	6.1682
	0.30	12.4816	8.5795	6.6629	4.6990	4.0275
Type 3	0	11.9653	9.3304	8.5830	8.2134	8.0005
	0.06	12.0742	9.2488	8.3884	7.9580	7.7634
	0.12	12.1943	9.1470	8.1370	7.6086	7.4390
	0.18	12.3277	9.0180	7.8024	7.1023	6.9601
	0.24	12.4765	8.8515	7.3391	6.2992	6.1545
	0.30	12.6438	8.6316	6.6595	4.7518	4.2520

Table 9
Frequencies of SSSS FGP (Case 2) plates versus k and ξ ($K_1 = 100, K_2 = 10$).

Type of PSEF	ξ	k				
		0	1	2	5	10
Type 1	0	6.4003	5.1731	4.8447	4.7018	4.6186
	0.06	6.4587	5.2035	4.8584	4.7102	4.6349
	0.12	6.5196	5.2349	4.8709	4.7157	4.6492
	0.18	6.5834	5.2672	4.8818	4.7172	4.6607
	0.24	6.6501	5.3005	4.8907	4.7133	4.6679
	0.30	6.7200	5.3348	4.8969	4.7018	4.6685
Type 2	0	6.3418	5.1561	4.8379	4.6995	4.6179
	0.06	6.4001	5.1875	4.8527	4.7088	4.6346
	0.12	6.4610	5.2198	4.8663	4.7150	4.6492
	0.18	6.5246	5.2532	4.8783	4.7170	4.6607
	0.24	6.5912	5.2875	4.8883	4.7133	4.6675
	0.30	6.6609	5.3229	4.8954	4.7015	4.6671
Type 3	0	6.3647	5.1563	4.8333	4.6934	4.6117
	0.06	6.4229	5.1871	4.8475	4.7025	4.6284
	0.12	6.4837	5.2188	4.8607	4.7086	4.6434
	0.18	6.5473	5.2516	4.8723	4.7108	4.6554
	0.24	6.6138	5.2853	4.8819	4.7076	4.6632
	0.30	6.6835	5.3200	4.8888	4.6969	4.6644

Table 10
Frequencies of CCCC FGP (Case 2) plates versus k and ξ ($K_1 = 100, K_2 = 10$).

Type of PSEF	ξ	k				
		0	1	2	5	10
Type 1	0	12.1780	9.4730	8.7037	8.3214	8.1013
	0.06	12.2843	9.5123	8.7017	8.3023	8.0965
	0.12	12.3954	9.5523	8.6951	8.2739	8.0846
	0.18	12.5115	9.5928	8.6827	8.2334	8.0630
	0.24	12.6332	9.6337	8.6632	8.1771	8.0277
	0.30	12.7607	9.6748	8.6347	8.0996	7.9730
Type 2	0	11.8029	9.2347	8.5091	8.1530	7.9476
	0.06	11.9065	9.2754	8.5110	8.1392	7.9477
	0.12	12.0148	9.3169	8.5088	8.1169	7.9413
	0.18	12.1280	9.3591	8.5014	8.0835	7.9261
	0.24	12.2466	9.4019	8.4874	8.0353	7.8982
	0.30	12.3709	9.4450	8.4653	7.9676	7.8524
Type 3	0	11.9653	9.3304	8.5830	8.2134	8.0005
	0.06	12.0700	9.3702	8.5827	8.1967	7.9978
	0.12	12.1794	9.4106	8.5780	8.1710	7.9883
	0.18	12.2938	9.4516	8.5678	8.1337	7.9695
	0.24	12.4136	9.4931	8.5507	8.0812	7.9376
	0.30	12.5391	9.5349	8.5251	8.0083	7.8870

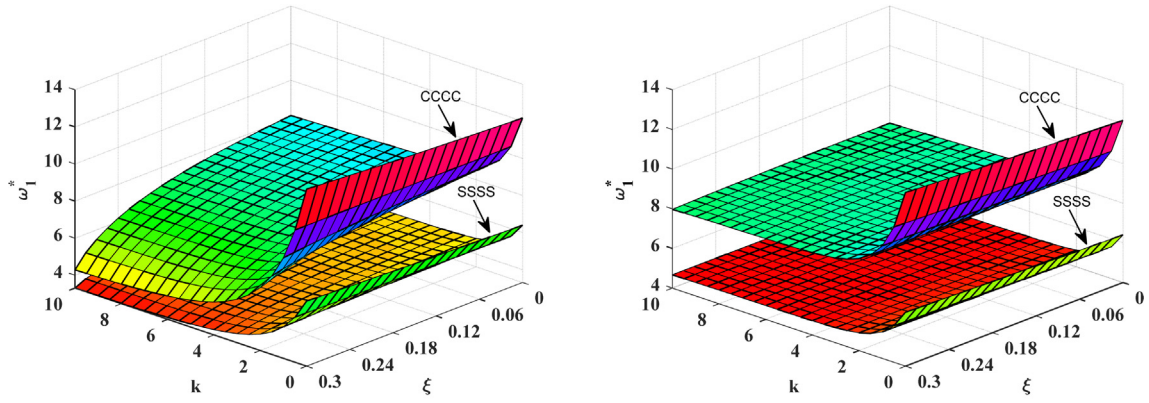

(a) Type 1, case 1

(b) Type 1, case 2

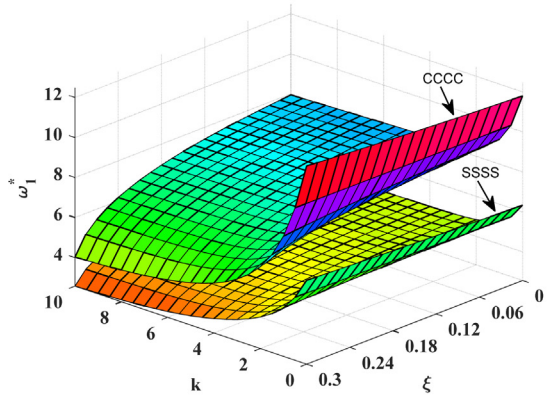

(c) Type 2, case 1

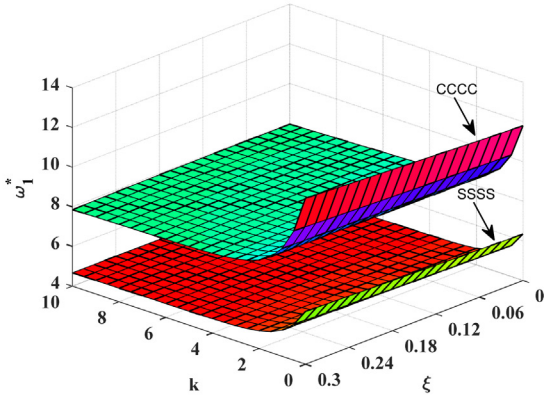

(d) Type 2, case 2

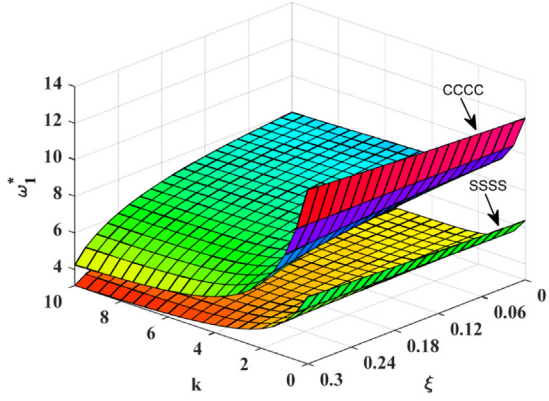

(e) Type 3, case 1

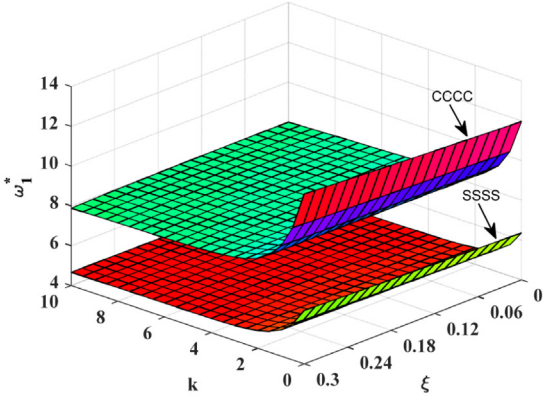

(f) Type 3, case 2

Fig. 13. Frequencies of FGP plates versus *k*and ξ. (a) Type 1; case 1, (b) Type 1; case 2, (c) Type 2; case 1, (d) Type 2; case 2, (e) Type 3; case 1, (f) Type 3; case 2.

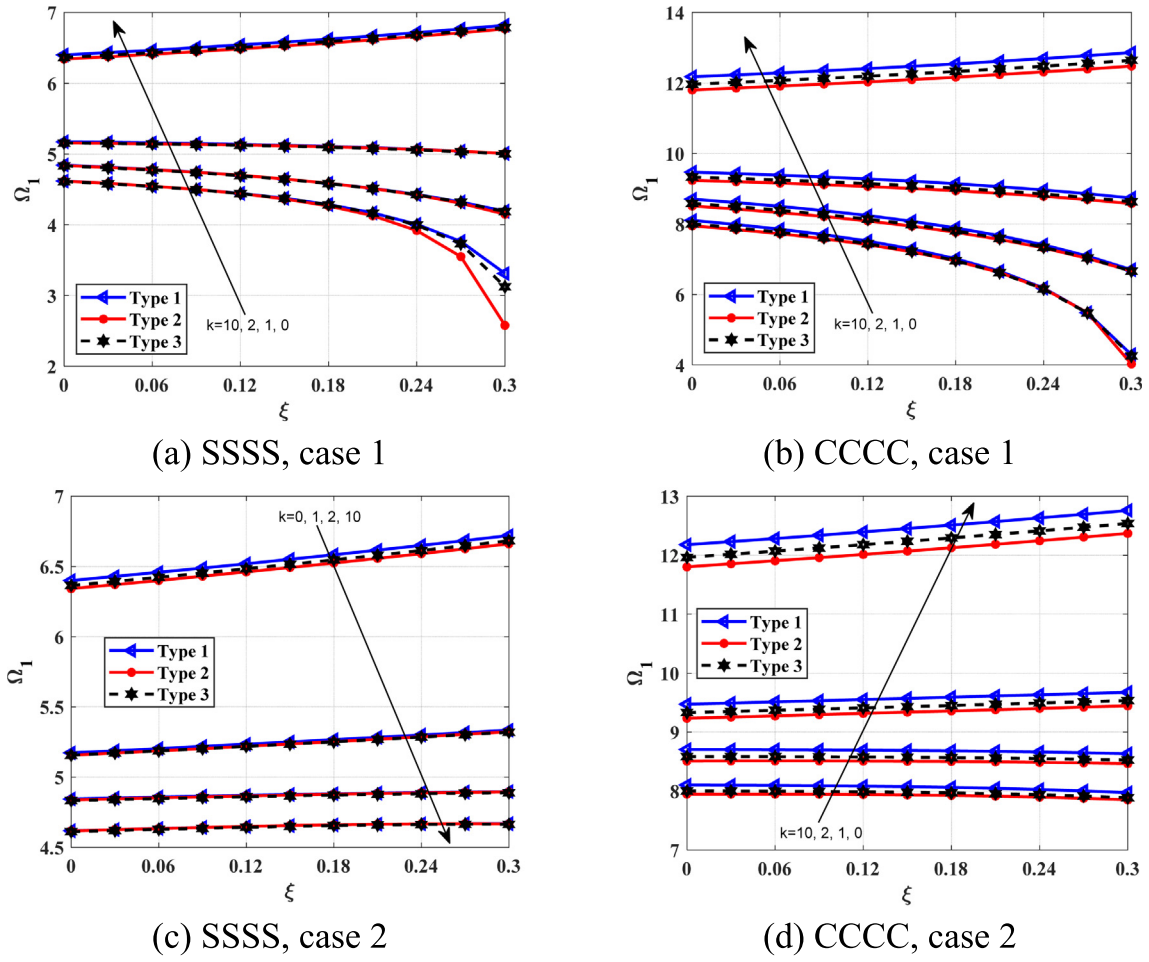

Fig. 14. Frequencies of FGP plates versus $\xi$with different values of k ($K_1 = 100, K_2 = 10$). (a) SSSS; case 1, (b) CCCC; case 1, (c) SSSS; case 2, (d) CCCC, case 2.

- The foundation stiffness parameters and material properties greatly influence the free vibration behavior of the plate. Adjusting these parameters can control the free vibration of FGP plates.
- This article provides initial results for further studies on the buckling and dynamic response of FGP plates located on PSEF using different plate theories.

7. Data availability

The data used to support the findings of this study is included in the article.

Declaration of Competing Interest

The authors declare that they have no known competing financial interests or personal relationships that could have appeared to influence the work reported in this paper.

Acknowledgements

The authors gratefully acknowledge the financial support granted by the Scientific Research Fund of Ho Chi Minh City Open University for this project.

References

[1] Bakoura A, Bourada F, Bousahla AA, Tounsi A, Benrahou KH, Tounsi A, et al. Buckling analysis of functionally graded plates using HSDT in conjunction with the stress function method. Comput Concr 2021;27(1):73–83.
[2] Zerrouki R, Karas A, Zidour M, Bousahla AA, Tounsi A, Bourada F, et al. Effect of nonlinear FG-CNT distribution on mechanical properties of functionally graded nano-composite beam. Struct Eng Mech 2021;78(2):117–24.
[3] Rabhi M, Benrahou KH, Kaci A, Houari MSA, Bourada F, Bousahla AA, et al. A new innovative 3-unknowns HSDT for buckling and free vibration of exponentially graded sandwich plates resting on elastic foundations under various boundary conditions. Geomech Eng 2020;22(2):119–32.
[4] Bekkaye THL, Fahsi B, Bousahla AA, Bourada F, Tounsi A, Benrahou KH, et al. Porosity-dependent mechanical behaviors of FG plate using refined trigonometric shear deformation theory. Comput Concr 2020;26(5):439–50.
[5] Zine A, Bousahla AA, Bourada F, Benrahou KH, Tounsi A, Adda Bedia E, et al. Bending analysis of functionally graded porous plates via a refined shear deformation theory. Comput Concr 2020;26(1):63–74.
[6] Tounsi A, Al-Dulaijan S, Al-Osta MA, Chikh A, Al-Zahrani M, Sharif A, et al. A four variable trigonometric integral plate theory for hygro-thermo-mechanical bending analysis of AFG ceramic-metal plates resting on a two-parameter elastic foundation. Steel Compos Struct 2020;34(4):511–24.
[7] Menasria A, Kaci A, Bousahla AA, Bourada F, Tounsi A, Benrahou KH, et al. A four-unknown refined plate theory for dynamic analysis of FG-sandwich plates under various boundary conditions. Steel Compos Struct 2020;36(3):355–67.
[8] Luat DT, Van Thom D, Thanh TT, Van Minh P, Van Ke T, Van Vinh P. Mechanical analysis of bi-functionally graded sandwich nanobeams. Adv Nano Res 2021;11(1):55–71.
[9] Shahsavari D, Shahsavari M, Li L, Karami B. A novel quasi-3D hyperbolic theory for free vibration of FG plates with porosities resting on Winkler/Pasternak/Kerr foundation. Aerosp Sci Technol 2018;72:134–49.
[10] Bansal G, Gupta A, Katiyar V. Vibration of porous functionally graded plates with geometric discontinuities and partial supports. Proc Instit Mech Eng, Part C: J Mech Eng Sci 2020;234(21):4149–70.
[11] Zenkour A. Quasi-3D refined theory for functionally graded porous plates: displacements and stresses. Phys Mesomech 2020;23(1):39–53.
[12] Barati MR, Zenkour AM. Electro-thermoelastic vibration of plates made of porous functionally graded piezoelectric materials under various boundary conditions. J Vib Control 2018;24(10):1910–26.
[13] Barati MR, Zenkour AM. Analysis of postbuckling of graded porous GPL-reinforced beams with geometrical imperfection. Mech Adv Mater Struct 2019;26(6):503–11.
[14] Daikh AA, Zenkour AM. Effect of porosity on the bending analysis of various functionally graded sandwich plates. Mater Res Express 2019;6(6):065703.
[15] Daikh AA, Zenkour AM. Free vibration and buckling of porous power-law and sigmoid functionally graded sandwich plates using a simple higher-order shear deformation theory. Mater Res Express 2019;6(11):115707.
[16] Heshmati M, Jalali S. Effect of radially graded porosity on the free vibration behavior of circular and annular sandwich plates. Eur J Mech-A/Solids 2019;74:417–30.
[17] Nguyen NV, Nguyen HX, Lee S, Nguyen-Xuan H. Geometrically nonlinear polygonal finite element analysis of functionally graded porous plates. Adv Eng Softw 2018;126:110–26.
[18] Nguyen NV, Lee J, Nguyen-Xuan H. Active vibration control of GPLs-reinforced FG metal foam plates with piezoelectric sensor and actuator layers. Compos B Eng 2019;172:769–84.
[19] Kumar R, Lal A, Singh B, Singh J. Meshfree approach on buckling and free vibration analysis of porous FGM plate with proposed IHHSDT resting on the foundation. Curv Layer Struct 2019;6(1):192–211.
[20] Rezaei A, Saidi A. Application of Carrera Unified Formulation to study the effect of porosity on natural frequencies of thick porous–cellular plates. Compos B Eng 2016;91:361–70.
[21] Rezaei A, Saidi A. Exact solution for free vibration of thick rectangular plates made of porous materials. Compos Struct 2015;134:1051–60.
[22] Zhao J, Xie F, Wang A, Shuai C, Tang J, Wang Q. A unified solution for the vibration analysis of functionally graded porous (FGP) shallow shells with general boundary conditions. Compos B Eng 2019;156:406–24.
[23] Zhao J, Xie F, Wang A, Shuai C, Tang J, Wang Q. Vibration behavior of the functionally graded porous (FGP) doubly-curved panels and shells of revolution by using a semi-analytical method. Compos B Eng 2019;157:219–38.
[24] Tran TT, Tran VK, Pham Q-H, Zenkour AM. Extended four-unknown higher-order shear deformation nonlocal theory for bending, buckling and free vibration of functionally graded porous nanoshell resting on elastic foundation. Compos Struct 2021;264:113737.
[25] Arshid E, Khorasani M, Soleimani-Javid Z, Amir S, Tounsi A. Porosity-dependent vibration analysis of FG microplates embedded by polymeric nanocomposite patches considering hygrothermal effect via an innovative plate theory. Eng Comput 2021:1–22.
[26] Kumar Y, Gupta A, Tounsi A. Size-dependent vibration response of porous graded nanostructure with FEM and nonlocal continuum model. Adv Nano Res 2021;11(1):1–17.
[27] Al-Furjan M, Habibi M, Ghabussi A, Safarpour H, Safarpour M, Tounsi A. Non-polynomial framework for stress and strain response of the FG-GPLRC disk using three-dimensional refined higher-order theory. Eng Struct 2021;228:111496.
[28] Tahir SI, Chikh A, Tounsi A, Al-Osta MA, Al-Dulaijan SU, Al-Zahrani MM. Wave propagation analysis of a ceramic-metal functionally graded sandwich plate with different porosity distributions in a hygro-thermal environment. Compos Struct 2021;269:114030.
[29] Al-Furjan M, Habibi M, Shan L, Tounsi A. On the vibrations of the imperfect sandwich higher-order disk with a lactic core using generalize differential quadrature method. Compos Struct 2021;257:113150.
[30] Guellil M, Saidi H, Bourada F, Bousahla AA, Tounsi A, Al-Zahrani MM, et al. Influences of porosity distributions and boundary conditions on mechanical bending response of functionally graded plates resting on Pasternak foundation. Steel Compos Struct 2021;38(1):1–15.
[31] Tahir SI, Tounsi A, Chikh A, Al-Osta MA, Al-Dulaijan SU, Al-Zahrani MM. An integral four-variable hyperbolic HSDT for the wave propagation investigation of a ceramic-metal FGM plate with various porosity distributions resting on a viscoelastic foundation. Waves Rand Compl Med 2021:1–24.
[32] Bellifa H, Selim MM, Chikh A, Bousahla AA, Bourada F, Tounsi A, et al. Influence of porosity on thermal buckling behavior of functionally graded beams. Smart Struct Syst 2021;27(4):719.
[33] Kaddari M, Kaci A, Bousahla AA, Tounsi A, Bourada F, Tounsi A, et al. A study on the structural behaviour of functionally graded porous plates on elastic foundation using a new quasi-3D model: bending and free vibration analysis. Comput Concr 2020;25(1):37–57.
[34] Tran V-K, Tran T-T, Phung M-V, Pham Q-H, Nguyen-Thoi T. A finite element formulation and nonlocal theory for the static and free vibration analysis of the sandwich functionally graded nanoplates resting on elastic foundation. J Nanomater 2020;2020.
[35] Pham Q-H, Tran TT, Tran VK, Nguyen P-C, Nguyen-Thoi T, Zenkour AM. Bending and hygro-thermo-mechanical vibration analysis of a functionally graded porous sandwich nanoshell resting on elastic foundation. Mech Adv Mater Struct 2021:1–21.
[36] Doan TL, Le PB, Tran TT, Trai VK, Pham QH. Free vibration analysis of functionally graded porous nano-plates with different shapes resting on elastic foundation (Articles in Press). J Appl Comput Mech 2021.
[37] Li Q, Wu D, Chen X, Liu L, Yu Y, Gao W. Nonlinear vibration and dynamic buckling analyses of sandwich functionally graded porous plate with graphene platelet reinforcement resting on Winkler-Pasternak elastic foundation. Int J Mech Sci 2018;148:596–610.
[38] Zenkour A, Radwan A. Free vibration analysis of multilayered composite and soft core sandwich plates resting on Winkler-Pasternak foundations. J Sandwich Struct Mater 2018;20(2):169–90.
[39] Duc ND, Bich DH, Cong PH. Nonlinear thermal dynamic response of shear deformable FGM plates on elastic foundations. J Therm Stresses 2016;39(3):278–97.
[40] Duc ND, Seung-Eock K, Cong PH, Anh NT, Khoa ND. Dynamic response and vibration of composite double curved shallow shells with negative Poisson's ratio in auxetic honeycombs core layer on elastic foundations subjected to blast and damping loads. Int J Mech Sci 2017;133:504–12.
[41] Duc N. Nonlinear static and dynamic stability of functionally graded plates and shells. Vietnam: Vietnam Natl Univ Press. Google Scholar; 2014.
[42] Mahmoudi A, Benyoucef S, Tounsi A, Benachour A, Adda Bedia EA, Mahmoud S. A refined quasi-3D shear deformation theory for thermo-mechanical behavior of functionally graded sandwich plates on elastic foundations. J Sandwich Struct Mater 2019;21(6):1906–29.

[43] Xiang Y, Wang C, Kitipornchai S. Exact vibration solution for initially stressed Mindlin plates on Pasternak foundations. Int J Mech Sci 1994;36(4):311–6.
[44] Omurtag MH, Özütok A, Aköz AY, OeZCELİKOeRS Y. Free vibration analysis of Kirchhoff plates resting on elastic foundation by mixed finite element formulation based on Gateaux differential. Int J Numer Meth Eng 1997;40 (2):295–317.
[45] Zhou D, Cheung Y, Lo S, Au F. Three-dimensional vibration analysis of rectangular thick plates on Pasternak foundation. Int J Numer Meth Eng 2004;59(10):1313–34.
[46] Ferreira A, Roque C, Neves A, Jorge R, Soares C. Analysis of plates on Pasternak foundations by radial basis functions. Comput Mech 2010;46(6):791–803.
[47] Merazka B, Bouhadra A, Menasria A, Selim MM, Bousahla AA, Bourada F, et al. Hygro-thermo-mechanical bending response of FG plates resting on elastic foundations. Steel Compos Struct 2021;39(5):631.
[48] Bendenia N, Zidour M, Bousahla AA, Bourada F, Tounsi A, Benrahou KH, et al. Deflections, stresses and free vibration studies of FG-CNT reinforced sandwich plates resting on Pasternak elastic foundation. Comput Concr 2020;26 (3):213–26.
[49] Bourada F, Bousahla AA, Tounsi A, Bedia E, Mahmoud S, Benrahou KH, et al. Stability and dynamic analyses of SW-CNT reinforced concrete beam resting on elastic-foundation. Comput Concr 2020;25(6):485–95.
[50] Tran TT, Pham Q-H, Nguyen-Thoi T. Dynamic Analysis of Functionally Graded Porous Plates Resting on Elastic Foundation Taking into Mass subjected to Moving Loads Using an Edge-Based Smoothed Finite Element Method. Shock Vib 2020;2020.
[51] Tran TT, Pham QH, Nguyen-Thoi T. Dynamic analysis of sandwich auxetic honeycomb plates subjected to moving oscillator load on elastic foundation. Adv Mater Sci Eng 2020;2020.
[52] Tran TT, Nguyen P-C, Pham Q-H. Vibration analysis of FGM plate in thermal environment resting on elastic foundation using ES-MITC3 element and prediction of ANN. Case Stud Therm Eng 2021:100852.
[53] Mudhaffar IM, Tounsi A, Chikh A, Al-Osta MA, Al-Zahrani MM, Al-Dulaijan SU. Hygro-thermo-mechanical bending behavior of advanced functionally graded ceramic metal plate resting on a viscoelastic foundation. In: Structures. Elsevier; 2021. p. 2177–89.
[54] Rouabhia A, Chikh A, Bousahla AA, Bourada F, Heireche H, Tounsi A, et al. Physical stability response of a SLGS resting on viscoelastic medium using nonlocal integral first-order theory. Steel Compos Struct 2020;37(6):695–709.
[55] Bellal M, Hebali H, Heireche H, Bousahla AA, Tounsi A, Bourada F, et al. Buckling behavior of a single-layered graphene sheet resting on viscoelastic medium via nonlocal four-unknown integral model. Steel Compos Struct 2020;34(5):643–55.
[56] Motaghian S, Mofid M, Akin JE. On the free vibration response of rectangular plates, partially supported on elastic foundation. Appl Math Model 2012;36:4473–82.
[57] Le CI, Pham VN, Nguyen DK. Free vibration of FGSW plates partially supported by Pasternak foundation based on refined shear deformation theories. Math Probl Eng 2020;2020.
[58] Wang X, Yuan Z, Jin C. Weak form quadrature element method and its applications in science and engineering: a state-of-the-art review. Appl Mech Rev 2017;69(3).
[59] Liu G-R. The smoothed finite element method (S-FEM): A framework for the design of numerical models for desired solutions. Front Struct Civ Eng 2019;13 (2):456–77.
[60] Nguyen-Thoi T, Liu G, Vu-Do H, Nguyen-Xuan H. An edge-based smoothed finite element method for visco-elastoplastic analyses of 2D solids using triangular mesh. Comput Mech 2009;45(1):23–44.
[61] Nguyen-Xuan H, Liu G, Nguyen-Thoi T, Nguyen-Tran C. An edge-based smoothed finite element method for analysis of two-dimensional piezoelectric structures. Smart Mater Struct 2009;18(6):065015.
[62] Tran TN, Liu G, Nguyen-Xuan H, Nguyen-Thoi T. An edge-based smoothed finite element method for primal–dual shakedown analysis of structures. Int J Numer Meth Eng 2010;82(7):917–38.
[63] Liu G-R, Trung N. Smoothed finite element methods. CRC Press; 2016.
[64] Liu G, Nguyen-Thoi T, Lam K. An edge-based smoothed finite element method (ES-FEM) for static, free and forced vibration analyses of solids. J Sound Vib 2009;320(4–5):1100–30.
[65] Lee P-S, Bathe K-J. Development of MITC isotropic triangular shell finite elements. Comput Struct 2004;82(11–12):945–62.
[66] Chau-Dinh T, Nguyen-Duy Q, Nguyen-Xuan H. Improvement on MITC3 plate finite element using edge-based strain smoothing enhancement for plate analysis. Acta Mech 2017;228(6):2141.
[67] Nguyen T-K, Nguyen V-H, Chau-Dinh T, Vo TP, Nguyen-Xuan H. Static and vibration analysis of isotropic and functionally graded sandwich plates using an edge-based MITC3 finite elements. Compos B Eng 2016;107:162–73.
[68] Tran TT, Pham Q-H, Nguyen-Thoi T. Static and free vibration analyses of functionally graded porous variable-thickness plates using an edge-based smoothed finite element method. Defence Technol 2021;17(3):971–86.
[69] Pham Q-H, Tran TT, Tran VK, Nguyen P-C, Nguyen-Thoi T. Free vibration of functionally graded porous non-uniform thickness annular-nanoplates resting on elastic foundation using ES-MITC3 element. Alexandr Eng J 2021.
[70] Thanh TT, Van Ke T, Hoa PQ, Trung NT. An edge-based smoothed finite element for buckling analysis of functionally graded material variable-thickness plates, Vietnam. J Mech 2021.
[71] Tran TT, Pham Q-H, Nguyen-Thoi T. An edge-based smoothed finite element for free vibration analysis of functionally graded porous (FGP) plates on elastic foundation taking into mass (EFTIM). Math Probl Eng 2020;2020.
[72] Nguyen-Thoi T, Phung-Van P, Nguyen-Xuan H, Thai-Hoang C. A cell-based smoothed discrete shear gap method using triangular elements for static and free vibration analyses of Reissner-Mindlin plates. Int J Numer Meth Eng 2012;91(7):705–41.
[73] Bletzinger K-U, Bischoff M, Ramm E. A unified approach for shear-locking-free triangular and rectangular shell finite elements. Comput Struct 2000;75 (3):321–34.
[74] Bathe KJ, Dvorkin EN. A formulation of general shell elements—the use of mixed interpolation of tensorial components. Int J Numer Meth Eng 1986;22 (3):697–722.
[75] Nguyen-Thoi T, Liu G, Nguyen-Xuan H. An n-sided polygonal edge-based smoothed finite element method (nES-FEM) for solid mechanics. Int J Num Meth Biomed Eng 2011;27(9):1446–72.
[76] Nguyen-Thoi T, Phung-Van P, Rabczuk T, Nguyen-Xuan H, Le-Van C. An application of the ES-FEM in solid domain for dynamic analysis of 2D fluid–solid interaction problems. Int J Comput Meth 2013;10(01):1340003.
[77] Nguyen-Thoi T, Phung-Van P, Ho-Huu V, Le-Anh L. An edge-based smoothed finite element method (ES-FEM) for dynamic analysis of 2D Fluid-Solid interaction problems. KSCE J Civ Eng 2015;19(3):641–50.
[78] Le CV, Nguyen-Xuan H, Askes H, Rabczuk T, Nguyen-Thoi T. Computation of limit load using edge-based smoothed finite element method and second-order cone programming. Int J Comput Methods 2013;10(01):1340004.
[79] Nguyen-Xuan H, Tran LV, Nguyen-Thoi T, Vu-Do H. Analysis of functionally graded plates using an edge-based smoothed finite element method. Compos Struct 2011;93(11):3019–39.
[80] Phan-Dao H, Nguyen-Xuan H, Thai-Hoang C, Nguyen-Thoi T, Rabczuk T. An edge-based smoothed finite element method for analysis of laminated composite plates. Int J Comput Methods 2013;10(01):1340005.
[81] Reddy JN. Mechanics of laminated composite plates and shells: theory and analysis. CRC Press; 2003.